Cellulose (2022) 29:469–481
https://doi.org/10.1007/s10570-021-04299-3

ORIGINAL RESEARCH

Graphene oxide and polyethyleneimine cooperative construct ionic imprinted cellulose nanocrystal aerogel for selective adsorption of Dy(III)

Xudong Zheng · Wen Sun · Ang Li · Bin Wang · Rong Jiang · Zhiqiang Song · Yuzhe Zhang · Zhongyu Li

Received: 30 August 2021 / Accepted: 27 October 2021 / Published online: 9 November 2021

Abstract Because of dysprosium's unique physical and chemical properties and limited supply, the price of rare earth dysprosium has been high in recent years. Therefore, the study of the method of high efficiency selective separation of dysprosium has the double value of scientific research and practical economy. In this paper, we used periodic cellulose nanocrystals as the basic structure, polyethylenimine and graphene oxide were introduced, combined with imprinting technology, to construct a porous imprinted aerogel and use it for selective adsorption of Dy(III). The physical and chemical properties were characterized by SEM, FT-IR and TGA. It was proved that both polyethylenimine and graphene oxide were cross-linked effectively with cellulose nanocrystals. Adsorption experiments showed that the composite imprinted aerogel could selectively adsorb dysprosium effectively, and the maximum adsorption capacity for Dy(III) was 36.495 mg g^{-1}. The reproducibility experiment showed that aerogel had good regeneration ability. In conclusion, cellulose nanocrystal aerogel, which is environmentally friendly, efficient and repeatable, is expected to provide a new direction for the recovery of rare earth elements.

Keywords Cellulose nanocrystal · Aerogel · Graphene oxide · Dysprosium · Adsorption

X. Zheng (✉) · W. Sun · A. Li · B. Wang · R. Jiang · Z. Song · Y. Zhang · Z. Li (✉)
School of Environmental and Safety Engineering, Changzhou University, Mingxing Building, Science and Education City, Wujin District, Changzhou 213164, Jiangsu, People's Republic of China
e-mail: zhengks@outlook.com

Z. Li
e-mail: zhongyuli@mail.tsinghua.edu.cn

Z. Li
Jiangsu Key Laboratory of Advanced Catalytic Materials and Technology, School of Petrochemical Engineering, Changzhou University, Mingxing Building, Science and Education City, Wujin District, Changzhou 213164, Jiangsu, People's Republic of China

Z. Li
Advanced Catalysis and Green Manufacturing Collaborative Innovation Center, Changzhou University, Mingxing Building, Science and Education City, Wujin District, Changzhou 213164, Jiangsu, People's Republic of China

Introduction

Rare earth elements, known as "industrial vitamins", are widely used in catalysts, permanent magnets, glassmaking, lighting and other fields (Liang et al., 2018; Huang and Zhu, 2019; Zhao et al., 2019; Ni'am et al., 2020). Dysprosium (Dy) has always been one of the most important rare earth elements because of its irreplaceable role in optics and permanent magnets (Fujiwara et al., 2016; Bisaka et al., 2017; Liang et al.,

2018; Zheng et al., 2020). Moreover, China has attached great importance to the rational development of rare earth resources in recent years. The price of rare earth has changed from "soil" to "rare". Therefore, it is of great significance for sustainable development to explore an economical and green separation and recovery technologies for dysprosium (Kaneko et al., 2019; Prodius et al., 2020).

Since the middle of the twentieth century, great efforts have been paid to the processing and recycling of dysprosium ions (Balaram, 2019; Habib, 2019). In various methods of recovering dysprosium ions, adsorption is an effective alternative because of its simplicity and cost-effectiveness (Kegl et al., 2019). Alcaraz (Alcaraz et al., 2019) synthesized two kinds of activated carbons from waste coffee grounds to adsorb and remove dysprosium ions in aqueous solution. Kaneko (Kaneko et al., 2019) synthesized MPS materials with high selective adsorption properties of dysprosium ions, which provided a new idea for the separation and recovery of dysprosium ions. However, since the similar physical and chemical properties of rare earth elements, it is a remaining major challenge to selectively adsorb of dysprosium. In addition, the cost of adsorption materials still restricts the industrial application of adsorption process. Therefore, the preparation of a low-cost adsorption material that can selectively adsorb dysprosium ions is our research goal.

Cellulose nanocrystals (CNCs) are considered as a kind of promising aerogel material due to their green, natural nature and low price (Almeida et al., 2018; Du et al., 2019; Zhang and Zhang, 2020). CNCs prepared by sulfuric acid hydrolysis usually have a diameter of 5–20 nm and a length of 10-hundreds of nanometers, and a large number of hydroxyl groups exist on their surfaces (George and S N, 2015; Kontturi et al., 2018). Since CNCs can form chiral nematic structures, the aerogel made by CNCs has a natural ordered pore structure (Xu et al., 2018), which is conducive to the occurrence of adsorption process (Sato et al., 2004; Kim et al., 2014; Cao et al., 2020). However, the physical and chemical properties of different rare earth ions are very similar, which greatly limits the separation of Dy(III) as a single element (Fang et al., 2021; Zhang et al., 2021). Therefore, we introduced the ionic imprinting technology to add more recognition sites on the surface of CNCs, so as to improve the high selectivity of adsorbents.

Due to its high specific surface area and porosity, aerogel is a very promising and ideal material in the field of adsorption (Du et al., 2013; Salimian et al., 2018), and has been applied in many scenarios, such as petroleum adsorbents. However, because the colloidal particles in the sol are usually randomly distributed, rapid drying of the gel to aerogel usually produces disordered networks (Long et al., 2018). The technology for preparing ordered aerogel is not well developed. To solve the problem, we introduced ordered CNCs and printed it into the aerogel material (Xu et al., 2018).

The branching end of polyethyleneimine (PEI) is rich in primary amine groups, which can easily form crosslinking points with other functional groups, so it is often used in the surface modification of nanomaterials (Zhao et al., 2017). Graphene oxide (GO) has lots of oxygen-containing groups such as carboxyl and hydroxyl groups on its surface, which have a good adsorption effect on Dy(III). At the same time, GO has the characteristics of high strength and good chemical stability, so cross-linking it with CNCs can improve the structural strength of aerogel (Ashour et al., 2017). In summary, we prepared a green imprinted GO-CNC-PEI aerogel (IGCPA) using CNCs as a framework, PEI and GO as bifocal monomers (Stepanova et al., 2019; Jiang et al., 2020), and combined with the ion imprinting technology for highly selective adsorption of Dy(III) (Fu et al., 2015).

Experimental section

Materials

Skimmed cotton was bought at a drugstore. Hydrochloric acid (HCl, 37%), Sulfuric acid (H_2SO_4, 98%), Nitric acid (HNO_3, 68%), Glacial acetic acid (CH_3COOH, 99.5%), Sodium hydroxide (NaOH, 96%), 2,2,6,6-Tetramethyl-1-piperidinyloxy (TEMPO, 97%), Ethanol (C_2H_5OH, 99.7%), Sodium bromide (NaBr, 99%) and Sodium hypochlorite (NaClO, Active chlorine $\geq$ 5.2%) were purchased from Sigma Aldrich. Dysprosium oxide (TREO $\geq$ 99.9%) was purchased from Shanghai Sinian Metal Materials Co., Ltd. Polyethyleneimine (PEI, 50%), 1-(3-Dimethylaminopropyl)-3-ethylcarbodiimide hydro (EDC, 98%) and N-Hydroxy succinimide (NHS, 98%) were bought from Aladdin Biochemical

Technology Co., Ltd. Graphene oxide solutions (GO, 10 mg mL^{-1}) were purchased from Nanjing Xianfeng Nanomaterials Technology Co., Ltd. The dysprosium nitrate ($Dy(NO_3)_3$) used in this study was prepared by dissolving dysprosium oxide with excessive concentrated nitric acid and reheating. The water used in this experiment was distilled water, and all reagents were not further purified unless otherwise specified.

Instruments

Scanning electron microscope (SEM, JEOL, Japan) was used to observe the surface morphology of the aerogel. The samples were tested by a Fourier transform infrared spectrophotometer (FT-IR, IS50, United States). Automatic specific surface and porosity analyzer (BET, ASAP 2460, USA) was used to analyze the specific surface area (S_{BET}) of aerogels. Under N_2 atmosphere, the aerogels were subjected to thermogravimetric analysis using a thermogravimetric analyzer (Q600-TGA/DSC, United States). The concentration of Dy(III) was measured by Inductively coupled plasma atomic emission spectrometer (ICP-OES, Vista-AX, United States).

Preparation of samples

The synthesis of CNC suspension 150 mL of H_2SO_4 was added to 150 mL of water, stirred evenly and cooled to room temperature. 20 g of skimmed cottons were put into the mixture, stirred it for 2 h at room temperature, then poured it into 3000 mL of ice water, and let it stand for 15 h for precipitation. The suspension of the lower phase was centrifuged and purified by dialysis until the pH value of the suspension was greater than 2.4.

The synthesis of TEMPO-CNC suspension After the CNC solution (100 mL, 4wt%) was evenly dispersed in 200 mL of water, 10 mg of TEMPO and 100 mg of NaBr were added to soak in the solution for 1 h. Added 40 mL of NaClO solution drop by drop, maintained a pH value of 10.5 with 0.1 M HCl and 0.1 M NaOH, and stirred for 4 h. Finally, 4 mL of C_2H_5OH was added to stop the oxidation reaction. 0.1 M HCl was used to adjust the solution to pH = 7.0. After standing overnight, dialysate was carried out and TEMPO-CNC suspension was obtained.

The synthesis of PEI-CNC aerogel 1000 mg of PEI (50%) was dispersed in 50 mL of TEMPO-CNC suspension, followed by ultrasonic for 30 min, then 250 mg of EDC and 250 mg of NHS were added into the mixed solution, stirred at room temperature for 24 h, and dialyzed to obtain a yellow suspension. After freeze drying, PEI-CNC aerogel was prepared.

The synthesis of GO-CNC-PEI aerogel (GCPA) 40 mg of GO was added to 20 mL of PEI-CNC suspension, the pH value was adjusted to 5.0 with 0.1 M HCl, and the solution was stirred for 3 h. GCPA was obtained by freeze-drying after dialysis purification.

The synthesis of IGCPA 40 mg of GO and 10 mg of $Dy(NO_3)_3$ were added to the 20 mL of PEI-CNC suspension, the pH value was adjusted to 5.0 by 0.1 M HCl and stirred for 3 h. Freeze drying after dialysis purification. Transferred the aerogel in an eluent (the volume ratio of glacial acetic acid to water was 1:9) for 48 h to remove Dy(III). Finally, the IGCPA was dried at room temperature after being rinsed three times with ultra-pure water. The preparation process and the possible adsorption mechanism of aerogel are shown in Figs. 1 and 2.

Adsorption experiment

Effect of pH on adsorption $Dy(NO_3)_3$ was used to prepare dysprosium ion original solution with a concentration of 50 mg L^{-1}. We took out 10 mL of original solutions and adjusted the pH value to 2.0, 3.0, 4.0, 5.0, 6.0 and 7.0 with 0.1 M HCl, respectively. Then we placed the solution in centrifuge tubes. 10 mg of adsorbents were then placed in a mixture of solutions in a centrifuge tube and allowed to sit for 24 h, maintaining the corresponding pH value of the solution. After the adsorption was completed, the mixture was centrifuged and the absorbents were removed using a 0.22 μm filter. The concentration of Dy(III) in the mixed solution was measured by the ICP-OES at a wavelength of 353.17 nm. The adsorption capacities Q_t (mg g^{-1}) were calculated by the following formula (Mahdi et al., 2018):

$$Q_t = \frac{V(C_0 - C_t)}{m} \quad (1)$$

where C_0 and C_t (mg L^{-1}) are the initial concentration and the residual concentration of Dy(III) in mixed solution, respectively. V (L) is the volume of Dy(III) stock solution, and m (g) is the mass of aerogel.

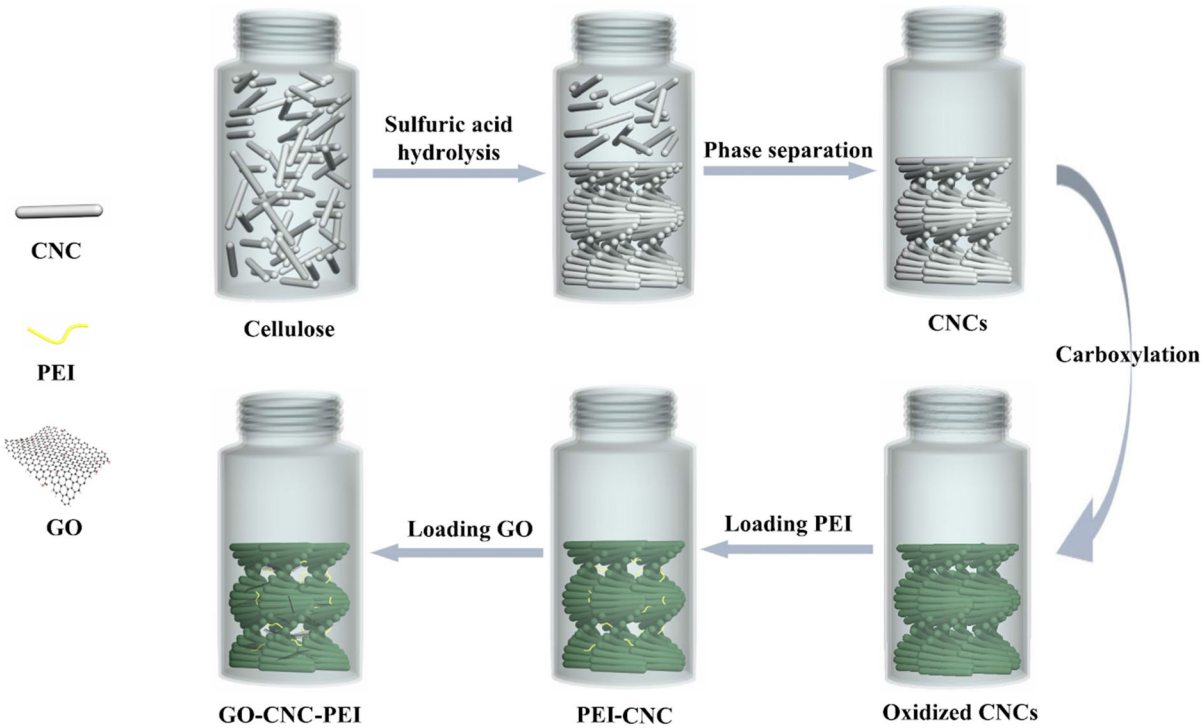

Fig. 1 Synthesis of cellulose nanocrystal aerogel

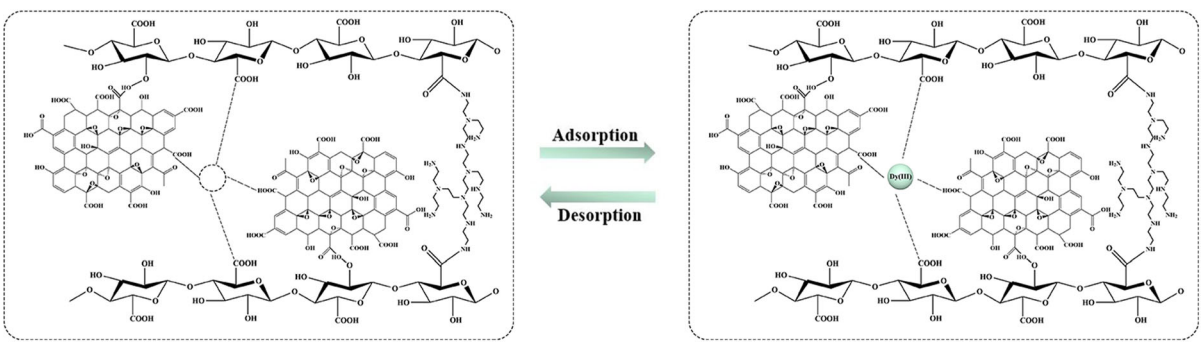

Fig. 2 Possible adsorption mechanism for Dy(III) onto IGCPA

Adsorption dynamics Three Dy(III) original solution (10 mL) was prepared, the pH was adjusted to 5.0, and placed in centrifuge tubes. Three kinds of aerogels (10 mg) were put into the tubes. The concentrations of dysprosium ions in mixed solution were determined at different contact times (0 min to 24 h). We used the software (Origin) to fit the adsorption kinetic data with the pseudo-first-order kinetic model (PFOKM, Eq. (2)) and the pseudo-second-order kinetic model (PSOKM, Eq. (3)) respectively, and then analyzed the adsorption mechanism (Wang et al., 2017).

$$Q_t = Q_e - Q_e e^{-k_1 t} \tag{2}$$

$$Q_t = \frac{k_2 Q_e^2 t}{1 + k_2 Q_e t} \tag{3}$$

where, Q_t (mg g^{-1}) and Q_e (mg g^{-1}) are the adsorption capacity of aerogels at time t and equilibrium, respectively. k_1 (min^{-1}) and k_2 (g mg^{-1} min^{-1}) represent the rate constants of PFOKM and PSOKM, respectively.

Adsorption isotherms Dy(III) solutions with concentrations of 0, 25, 50, 100, 150 and 200 mg L^{-1} were taken, adjusted to pH 5.0, and placed in centrifuge tubes. Three different kinds of aerogels (10 mg) were put into the mixed solutions. The adsorption of Dy(III) by aerogels at different values of initial concentrations was determined 24 h after the tubes were placed. Langmuir (Eq. (4)) and Freundlich (Eq. (5)) models were used to fit the experimental equilibrium data (Zhu et al., 2018).

$$Q_e = \frac{K_L Q_m C_e}{1 + K_L C_e} \tag{4}$$

$$Q_e = K_F C_e^{1/n} \tag{5}$$

C_e (mg L^{-1}) is the concentration of Dy(III) in solution at equilibrium, Q_m (mg g^{-1}) is the maximum adsorption capacity of aerogels for Dy(III). K_L (L mg^{-1}) is the Langmuir parameter denoted the energy of adsorption and affinity of binding sites. K_F (mg g^{-1}) is the Freundlich sorbent adsorption strength, while 1/*n* is the heterogeneity factors.

Adsorption thermodynamics 10 mg of aerogels were immersed in Dy(III) stock solution (10 mL, pH = 5.0) with different initial concentrations (25, 50, 100 mg L^{-1}). Adsorption tests were carried out at 288.15 K, 298.15 K and 308.15 K, respectively. The residual Dy(III) concentrations in the solution were determined after 24 h. The values of Gibbs energy (ΔG°) are calculated by equation Eq. (6) (Zhang et al., 2019):

$$\Delta G^{\circ} = -RT \ln K^{\circ} \tag{6}$$

where thermodynamic equilibrium constant K° is only a function of temperature. It is a constant of dimension 1, in units of "1". It's the vertical intercept of the linear equation of $\ln(C_s/C_e)$ and C_s. Wherein, C_s (mmol g^{-1}) is the adsorption amount per gram of aerogels, and C_e is the concentration of Dy(III) in the mixed solution at adsorption equilibrium. *R* (8.314 J mol^{-1} K^{-1}) is the universal gas constant, and *T* is the given temperature. Eventually, entropy (ΔS°) and the enthalpy (ΔH°) values are obtained from van't Hoff equation Eq. (7) (Zheng et al., 2020):

$$\ln K^{\circ} = \frac{\Delta S}{R} - \frac{\Delta H}{RT} \tag{7}$$

Selective tests 10 mg of aerogels were immersed in 10 mL of mixed solution with coexisting system (Dy(III), Nd(III) and Pr(III) were provided by $Dy(NO_3)_3$, $Nd(NO_3)_3$ and $Pr(NO_3)_3$ respectively). The initial concentration of each cation was 50 mg L^{-1}, and the pH value was adjusted to 5.0 with 0.1 M HCl. The concentration in the mixed solution was measured 24 h after the tubes were placed at 25 °C. The selectivity of aerogels was evaluated by K_d (mL g^{-1}). Relationships are listed as follows (Eq. (8)) (Sun et al., 2017):

$$K_d = \frac{V(C_0 - C_f)}{mC_f} \tag{8}$$

where, C_0 and C_f are the initial and final concentration of each rare earth ion, respectively. The C_0 of each cation is 50 mg L^{-1}.

Reusability tests After each adsorption process, the aerogels were separated from the solution by elution (10% glacial acetic acid solution) for 24 h to remove the adsorbed Dy(III). These aerogels were reused for adsorption experiments. We took stock solutions (50 mg L^{-1}), adjusted the pH to 5.0, and placed in a centrifuge tube. The adsorbents were then put into the solution. The residual concentration of Dy(III) in the solution was determined after 24 h at 25 °C. The whole adsorption–desorption experiment was repeated 5 times. The reusability of the aerogels was verified by the changes of five adsorption capacities of the aerogels.

Results and discussion

Aerogel characterization

SEM analysis The microstructure and surface morphology of composite aerogels were observed by scanning electron microscopy (SEM), as shown in Fig. 3. Under the combined action of GO and PEI, the materials showed the good porous structure. It could be seen that the material was composed of a large number of pores, which contributed to the ultra-light performance of the aerogels and also provided lots of adsorption sites for Dy(III) adsorption. The pores on the surface of PEI-CNC aerogel, GCPA and IGCPA all had good periodicity, which indicated that the composite aerogels could effectively replicate the structure of CNCs, the subsequent modification and the elution of imprinted ions had no effect on the

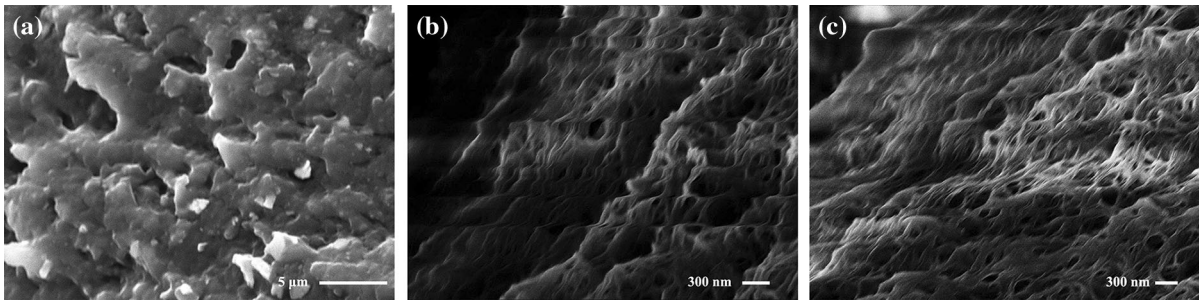

Fig. 3 SEM images of PEI-CNC aerogel (**a**), GCPA (**b**) and IGCPA (**c**)

structure of aerogels, which effectively maintained the periodicity template of the materials. In addition, in Fig. 3b, c, PEI and GO were uniformly distributed on the porous network of CNCs, indicating that the cross-linking between PEI and GO and CNCs was stable. The adhesion of GO to CNCs not only added additional adsorption sites, but also prevented the agglomeration of CNCs to a certain extent, which contributed to the efficient adsorption of Dy(III) by the adsorbent.

BET analysis The N_2 adsorption–desorption analysis isotherms are shown in Fig. 4 and Table 1. It could be seen from the isotherm fitting curve that the three kinds of aerogels adsorption processes all belonged to type IV. When the relative pressure was the low-pressure region (0.0–0.3 P/P_0), the upward curve was a monolayer adsorption process. When the monolayer adsorption reached saturation, the multilayer adsorption began. As the pressure increased, the pore size of the aggregate expanded, resulting in the subsequent phenomenon. The curves of adsorption return line adsorption and desorption formed were very steep, and the relative pressure of condensation and evaporation was in the middle. Therefore, the surface of IGCPA is a cylindrical hole with openings at both ends, which is consistent with the results of SEM images. In addition, the S_{BET} of PEI-CNC, GCPA and IGCPA were 4.175, 10.832 and 14.372 $m^2\ g^{-1}$, respectively. With the further functionalization of CNCs by PEI and GO, the S_{BET} of the material increased and the pore size became smaller, this might be due to the new pores generated on the surface of the CNCs. The small pores in the eluted IGCPA collapsed to form large pores, which caused the S_{BET} of the aerogel to become larger and the pore size also increased. In addition, the specific surface area of composite aerogels was generally smaller, most likely due to the formation of large aggregates or aggregates during drying (Peng et al., 2011; Brinkmann et al., 2016; Zheng et al., 2020).

Table 1 The pore structure parameters of four aerogels

Sample	Surface area (cm^2/g)	Pore size (nm)
PEI-CNC	4.1750	24.836
GCPA	10.832	12.589
IGCPA	14.372	19.779

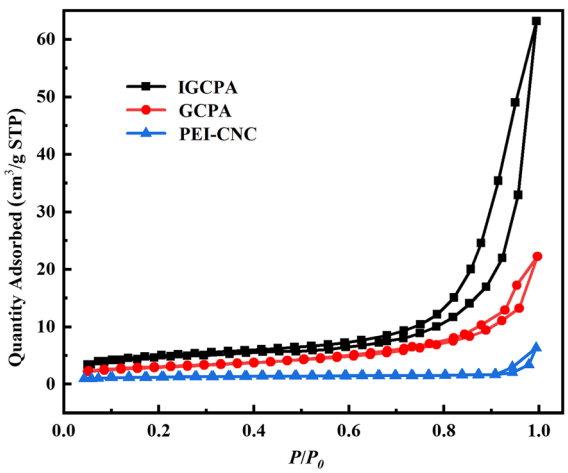

Fig. 4 N_2 adsorption–desorption isotherms of PEI-CNC, GCPA and IGCPA

FT-IR analysis Infrared spectra were measured, and FT-IR spectra of TEMPO-CNC after freeze drying and three aerogels are shown in Fig. 5. It is worth noting that the spectrum of TEMPO-CNC had a strong peak at 1627 cm^{-1}, which was a characteristic peak of the carbonyl of the carboxylic acid groups. There were three strong peaks in PEI-CNC spectrum at 1644, 1567

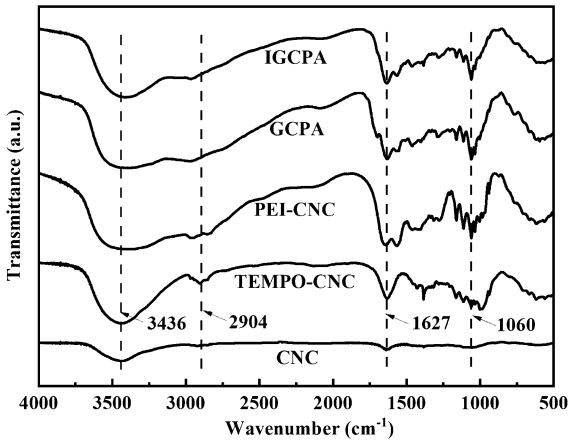

Fig. 5 FT-IR spectra of aerogels

and 1461 cm^{-1}, indicating the characteristic peaks of amide bond and an amino group. In addition, PEI-CNC showed a strong spectral band in the range of 3100–3550 cm^{-1}, which was due to the stretching vibration of O–H and N–H at 3100–3500 cm^{-1}. Therefore, it could be proved that the amino group has been successfully introduced in the cross-linking process of PEI. The peaks of GCPA and IGCPA at 2904 cm^{-1} were observed to change, which was attributed to the stretching vibration of -CH_2 due to defects in the graphite structure. It could be concluded that GO was successfully introduced into GCPA and IGCPA. In addition, the peaks of eluted IGCPA were consistent with that of GCPA, indicating that imprinted ions in IGCPA were completely washed and other groups remained stable, which proved that the modified material had good stability.

TG/DTG analysis The thermal stability of the material was investigated by increasing the temperature from 30 °C to 800 °C in N_2 atmosphere. The thermogravimetric results are shown in Fig. 6. When the temperature reaches 250 °C, the decomposition was obvious and the mass decreased by 15–25%, which was mainly due to water loss. The total mass loss between 250–400 °C could be explained by the decomposition of the nanofiber network structure. Above 400°C, entering the final carbonization stage, the mass loss gradually stopped, the TGA curve flattened out, and the residue was mainly composed of carbon left by calcination. The above results showed that the addition of GO, PEI and other materials improved the thermal stability of the materials. The total mass loss rate of IGCPA was less than that of GCPA, indicating that the imprinted aerogel had better thermal stability.

Analysis of adsorption results

Effect of pH on adsorption The pH value affects the presence of cations in the solution and the surface charge of the adsorbent. In order to avoid Dy^{3+} from forming dysprosium hydroxide precipitation under alkaline conditions, the adsorption properties in the pH range of 2.0–7.0 were studied. As can be seen from Fig. 7, with the increase of pH value, the adsorption amount of each adsorbent gradually increases. The adsorption capacity increased rapidly in the pH 1.0–5.0 range. When the pH value was higher than 5.0, the adsorption capacity gradually stabilized, which could be attributed to the low degree of dissociation of the -COOH group. In addition, the adsorption capacity of the non-imprinted aerogel was much lower than that of the imprinted aerogel. The imprinted factor (IF) defines the adsorption capacity ratio of the imprinted and non-imprinted aerogel and shows the separation capacity of the aerogels. When pH = 5.0, the maximum value was 1.420, and the imprinted aerogel could achieve the highest adsorption capacity. Therefore, in subsequent adsorption experiments, we set the pH = 5.0.

Adsorption dynamics The relationship between the adsorption quantity (Q_t) and contact time (t) was discussed by adsorption dynamics experiments. As can be seen from Fig. 8, the adsorption curve of aerogels grew rapidly at the beginning and reached 80% of the maximum adsorption capacity within 200 min. Then, the adsorption curve grew slowly and finally reached an adsorption equilibrium within 6 h, at which time the blot sites on the aerogels became saturated. The adsorption capacity of GCPA and IGCPA introduced with GO was significantly higher than that of PEI-CNC, and IGCPA had higher adsorption equilibrium than GCPA due to its unique imprinted hole. The PFOKM and PSOKM were fit the kinetic data to investigate the adsorption rate constant and adsorption mechanism. The relevant calculation parameters of the adsorption kinetics model are shown in Table 2. Obviously, the PSOKM model ($R^2 \geq 0.990$) and the kinetic data fit well, indicating that the main adsorption process was a chemical adsorption.

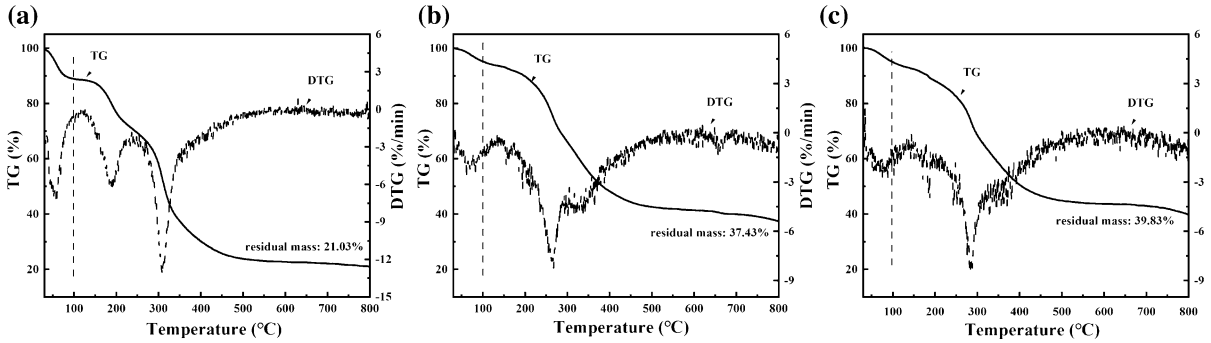

Fig. 6 TGA curves of PEI-CNC (**a**), GCPA (**b**) and IGCPA (**c**)

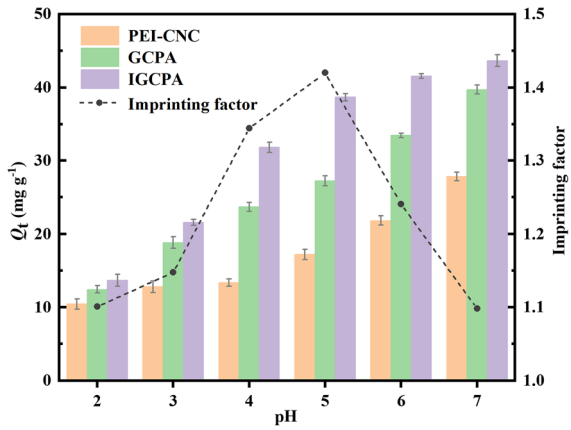

Fig. 7 Effect of pH on the adsorption properties of PEI-CNC, GCPA, IGCPA

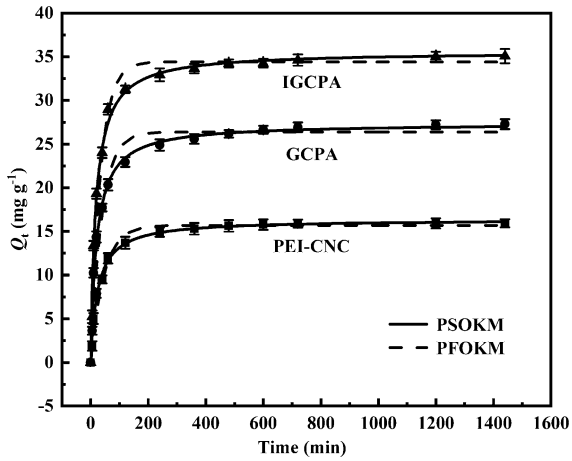

Fig. 8 Kinetic data and modeling for the adsorption of Dy(III)

Adsorption isotherm By contacting the Dy(III) solution with different initial concentration (0–200 mg L^{-1}), the differences of Dy(III) adsorption by different aerogels were analyzed, as well as the equilibrium data and adsorption curves. Langmuir isothermal model and Freundlich isothermal model were used to fit the experimental data of aerogels. As shown in Fig. 9, the adsorption capacity increased synchronously with the increase of the initial Dy(III) concentration. The maximum adsorption capacities of GCPA and IGCPA were 26.678 and 36.495 mg g^{-1}, respectively. Its high adsorption capacity was attributed to the functionalization of CNCs by GO and PEI, which provided more binding sites for Dy(III). Table 3 summarizes the relevant isothermal constants. The larger R^2 value (0.991–0.999) indicated that the Langmuir isothermal adsorption model could fit the experimental data well, and the adsorption process by aerogels proved to be a monolayer adsorption. The lower value of 1/*n* indicates that IGCPA has better adsorption conditions for Dy(III) than GCPA.

Adsorption thermodynamics The effects of three kinds of aerogels on the adsorption at different temperatures (288.15 K, 298.15 K and 308.15 K) were studied. ΔG° was calculated according to the Gibb's free energy change equation (Fig. 10), and ΔH° and ΔS° were obtained by the relation between $\ln K^{\circ}$ and $1/T$ (Fig. 11). Table 4 lists the thermodynamics related parameters of three aerogels. ΔG° was negative between -5.363 and − 6.742 kJ mol^{-1}, indicating that the adsorption of Dy(III) was spontaneous, and the higher the temperature, the more favorable the adsorption process. ΔH° was positive, indicating that the adsorption process was endothermic, which proved again that the increase of temperature was conducive to adsorption. ΔS° was positive, indicating that the adsorption process was an entropy increase process. In summary, the adsorption of Dy(III) by aerogels was spontaneous, endothermic and entropy-enhancing.

Table 2 Kinetic constants for the Pseudo-first-order and Pseudo-second-order models

Sorbents	Pseudo-first-order kinetic model			Pseudo-second-order kinetic model		
	Q_e (mg g^{-1})	$k_1 \times 10^{-2}$ (min^{-1})	R^2	Q_e (mg g^{-1})	$k_2 \times 10^{-2}$ (g mg^{-1} min^{-1})	R^2
PEI-CNC	15.429	2.809	0.981	16.372	0.250	0.993
GCPA	25.878	3.357	0.970	27.391	0.179	0.990
IGCPA	33.771	3.760	0.984	35.601	0.157	0.990

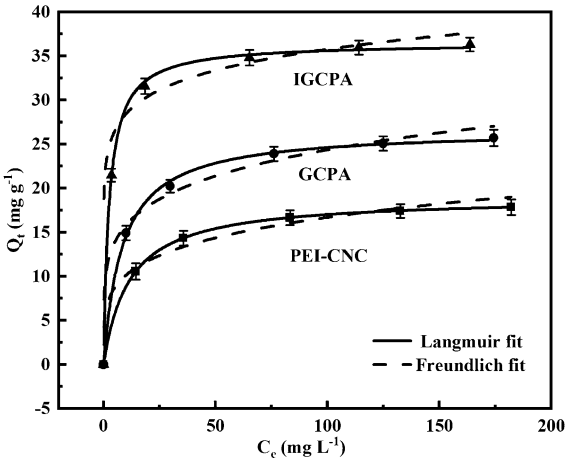

Fig. 9 Adsorption isotherm of Dy(III) by aerogels

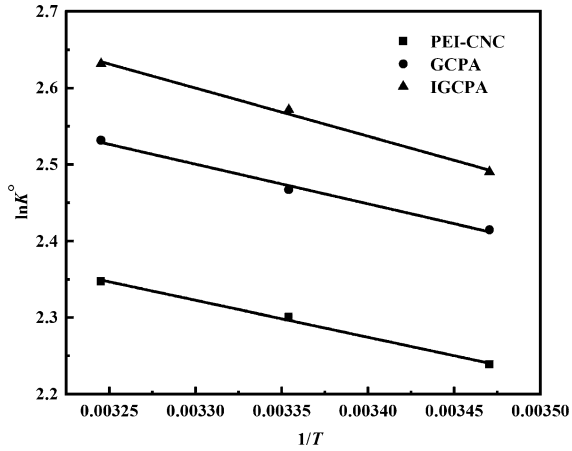

Fig. 11 Thermodynamic properties of three aerogels at different temperatures: $\ln K^{\circ}$ degrees versus $1/T$

Selective tests In order to prove that IGCPA has good adsorption selectivity, a competitive adsorption experiment was carried out. The imprinted aerogel adsorbed Dy(III) as well as Pr(III) and Nd(III). The result is shown in Fig. 12 and Table 5. The K_d value reflects adsorption selectivity of adsorbents for

Table 3 Adsorption equilibrium constants for Langmuir and Freundlich isotherm equations

Sorbents	Langmuir			Freundlich		
	Q_m (mg g^{-1})	K_L (L mg^{-1})	R^2	K_F (mg g^{-1})	$1/n$	R^2
PEI-CNC	18.972	0.0869	0.999	6.157	0.217	0.894
GCPA	26.678	0.119	0.991	10.243	0.188	0.871
IGCPA	36.495	0.397	0.994	22.557	0.100	0.744

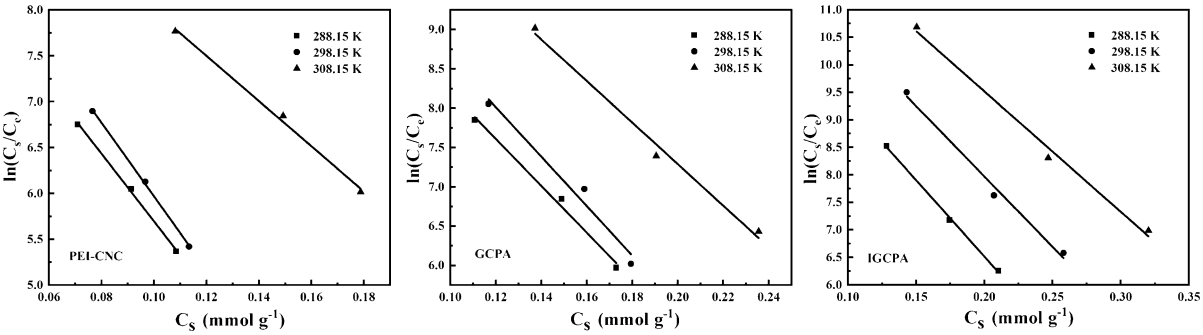

Fig. 10 Thermodynamic properties of three aerogels at different temperatures: a plot of $\ln(C_s/C_e)$

Table 4 Thermodynamic parameters of three aerogels

Sorbents	ΔH° (kJ mol^{-1})	ΔS° (J mol^{-1})	T (K)	K°	ΔG° (kJ mol^{-1})	R^2
PEI-CNC	4.011	32.547	288.15	9.382	− 5.363	0.993
			298.15	9.979	− 5.702	
			308.15	10.457	− 6.014	
GCPA	4.313	35.023	288.15	11.188	− 5.785	0.990
			298.15	11.789	− 6.116	
			308.15	12.577	− 6.487	
IGCPA	5.228	38.869	288.15	12.064	− 5.966	0.991
			298.15	13.086	− 6.374	
			308.15	13.897	− 6.742	

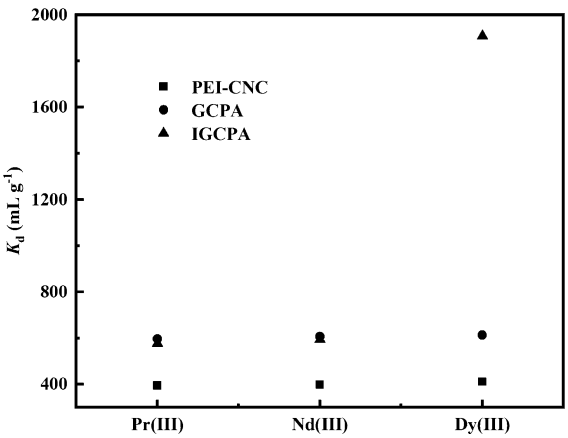

Fig. 12 The K_d values of different ions adsorbed by aerogels

Dy(III). The K_d value of IGCPA for Dy(III) was higher than that of GCPA, the maximum K_d value was 1909.2 mL g^{-1} of IGCPA. It could be seen that the unique imprinted hole on IGCPA had a specific adsorption on Dy(III), and this site could not adsorb other rare earth ions. Compared with other adsorption experiments, the total adsorption capacity of IGCPA for the three rare earth ions was higher than that of single dysprosium ion, which indicated that IGCPA could also adsorb Nd(III) and Pr(III). In this experiment, the adsorption capacity of IGCPA for Dy(III) decreased, indicating that other rare earth ions could interfere with the adsorption of Dy(III). According to Pearson's law, this was because Dy(III), Nd(III) and Pr(III) are all hard Lewis acids, and the strongest ion competition often occurs between the same type of metals. In addition, the results showed that the order of adsorption capacity was Dy(III) > Nd(III) > Pr(III). We speculate that this was related to the ion radius. The smaller the radius, the stronger the chelating ability of the metal ion to the carboxyl group. In summary, IGCPA could preferentially separate Dy(III) from the multi-ion coexistence system.

Regeneration The reuse of adsorbents will minimize industrial production costs. As can be seen from Fig. 13, five adsorption cycles were performed to test the reliability of the aerogels. After 5 cycles, the adsorption capacity decreased to 67.97–79.75% of the initial adsorption capacity, which was mainly due to the loss of adsorption sites caused by eluent elution, and the SEM image of IGCPA was basically the same as before the test. In conclusion, IGCPA has a reliable repeatability and is expected to be a commercially available adsorption material. Further, some other

Table 5 The K_d value of Dy(III) adsorbed by aerogels in mixed solution

Cation	PEI-CNC		GCPA		IGCPA	
	C_f (mg L^{-1})	K_d (mL g^{-1})	C_f (mg L^{-1})	K_d (mL g^{-1})	C_f (mg L^{-1})	K_d (mL g^{-1})
Pr(III)	35.874	393.77	31.707	597.09	31.718	576.39
Nd(III)	35.779	397.47	31.121	606.63	31.379	593.42
Dy(III)	35.456	410.20	31.003	612.75	17.187	1909.2

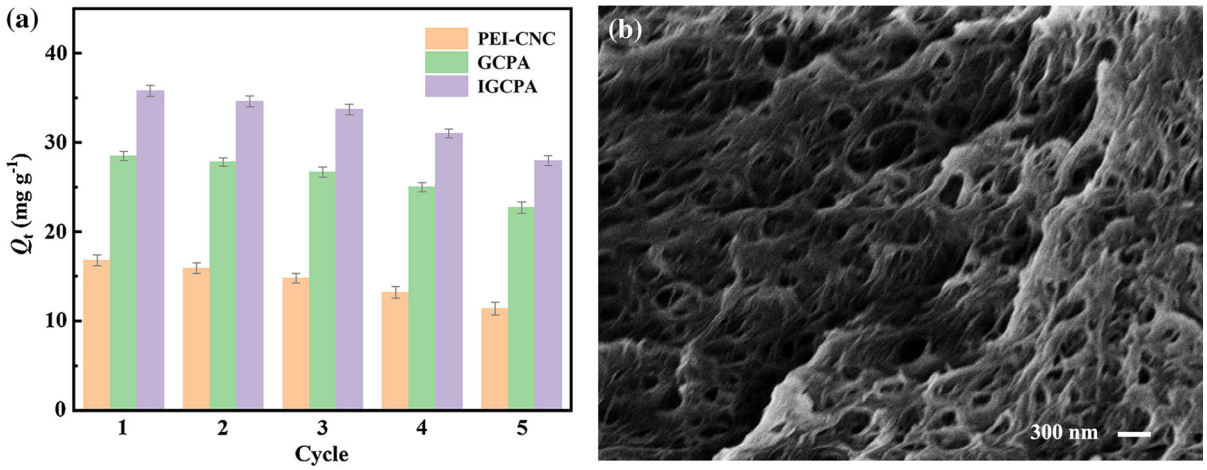

Fig. 13 Regeneration of aerogels and the SEM image of IGCPA over 5 cycles

Table 6 Comparison of IGCPA with those described in other literature

Sorbents	Cation	pH	Adsorption capacity (mg g^{-1})	References
IGCPA	Dy(III)	5.0	36.495	This study
o-CNCs/GO-IIPs	Dy(III)	4.0	41.790	(Zheng et al., 2020)
Imprinted mesoporous silica materials	Dy(III)	2.0	22.330	(Zheng et al., 2016)
Imprinted mesoporous cellulose films	Nd(III)	4.0	22.610	(Zheng et al., 2019)
PEI-cross-linked CNC (PEI-CNC)	Er(III)	5.4	120.29	(Zhao et al., 2017)

adsorbents were listed to compare adsorption capacities for REEs in Table 6 (Zheng et al., 2016, 2019, 2020; Zhao et al., 2017).

Conclusion

In this study, under the circumstance of environmental pollution caused by rare earth elements and the urgent need to reduce the cost, the imprinted aerogel IGCPA with periodic structure was prepared from biodegradable cellulose nanocrystals and used for the specific adsorption of Dy(III) in rare earth waste. GO and PEI were uniformly distributed on the CNC skeleton and did not affect the crystallization zone. The carboxyl group introduced by surface modification further improved the adsorption capacity of Dy(III) as a synergistic functional monomer. The results showed that the optimum pH value for adsorption was 5.0. PSOKM could fit the adsorption data well, indicating that aerogel adsorption of Dy(III) was mainly a chemical process. According to the adsorption isotherm, the adsorption process was mainly monolayer adsorption, and the maximum adsorption capacity was 36.495 mg g^{-1}. In multi-ion coexisting systems, the imprinted aerogel tended to adsorb Dy(III). In addition, the repeated use test showed that the material had a strong regeneration performance. The results showed that the composite imprinted aerogel could adsorb Dy(III) efficiently and greenly.

Acknowledgments The authors thank the National Natural Science Foundation of China (Grant Nos. 21876015, 21808018, 21878026, 22008014), Postgraduate Research & Practice Innovation Program of Jiangsu Province (No. KYCX20_2579, No. KYCX20_2592 and No. KYCX20_2595). Also, the author would like to thank the researchers at the Analytical Testing Center of Changzhou University for their assistance in SEM, FTIR and TG analysis.

Declarations

Conflict of interest The authors declare that they have no conflict of interest.

Ethical approval The article does not contain any experiments with human participants or animals performed by any of the authors.

Informed consent Informed consent was obtained from all individual participants included in the study.

References

Alcaraz L, Escudero ME, Alguacil FJ, Llorente I, Urbieta A, Fernández P, López FA (2019) Dysprosium Removal from Water Using Active Carbons Obtained from Spent Coffee Ground. Nanomaterials 9

Almeida APC, Canejo JP, Fernandes SN, Echeverria C, Almeida PL, Godinho MH (2018) Cellulose-Based Biomimetics and Their Applications. Adv Mater 30:1703655

Ashour RM, Abdelhamid HN, Abdel-Magied AF, Abdel-Khalek AA, Ali MM, Uheida A, Muhammed M, Zou X, Dutta J (2017) Rare earth ions adsorption onto graphene oxide nanosheets. Solvent Extr Ion Exc 35:91–103

Balaram V (2019) Rare earth elements: A review of applications, occurrence, exploration, analysis, recycling, and environmental impact. Geosci Front 4:1285–1303

Bisaka K, Thobadi IC, Pawlik C (2017) Extraction of rare earths from iron-rich rare earth deposits. J S Afr I Min Metall 117:731–739

Brinkmann A, Chen M, Couillard M, Jakubek ZJ, Leng T, Johnston LJ (2016) Correlating Cellulose Nanocrystal Particle Size and Surface Area. Langmuir 32:6105–6114

Cao Y, Wang PX, D'Acierno F, Hamad WY, Michal CA, MacLachlan MJ (2020) Tunable diffraction gratings from biosourced lyotropic liquid crystals. Adv Mater 32(19):1907376

Du A, Zhou B, Zhang Z, Shen J (2013) A special material or a new state of matter: a review and reconsideration of the aerogel. Materials 6:941–968

Du H, Liu W, Zhang M, Si C, Zhang X, Li B (2019) Cellulose nanocrystals and cellulose nanofibrils based hydrogels for biomedical applications. Carbohyd Polym 209:130–144

Fang L, Miao Y, Wei D, Zhang Y, Zhou Y (2021) Efficient removal of norfloxacin in water using magnetic molecularly imprinted polymer. Chemosphere 262:128032

Fu J, Chen L, Li J, Zhang Z (2015) Current status and challenges of ion imprinting. J Mater Chem A 3:13598–13627

Fujiwara I, Takeuchi K, Murakami Y (2016) Development of a Dysprosium (III) Ion-selective Electrode Using a Dysprosium (III)-imprinted Polymer. Bunseki Kagaku 65:527–531

George J, Sabapathi NS (2015) Cellulose nanocrystals: synthesis, functional properties, and applications. Nanotechnol Sci Appl

Habib K (2019) A products classification approach to optimize circularity of critical resources-the case of NdFeB magnets. J Clean Prod 230:90–97

Huang H, Zhu JJ (2019) The electrochemical applications of rare earth-based nanomaterials. Analyst 144:6789–6811

Jiang W, Shen P, Yi J, Li L, Wu C, Gu J (2020) Surface modification of nanocrystalline cellulose and its application in natural rubber composites. J Appl Polym Sci 137:49163

Kaneko T, Hikosaka R, Nagata F, Inagaki M, Kato K (2019) Effective adsorption of dysprosium ions on amino and carboxyl functionalized mesoporous silica sheets. J Asian Ceram Soc 7:213–220

Kegl T, Ban I, Lobnik A, Košak A (2019) Synthesis and characterization of novel γ-Fe_2O_3-NH_4OH@SiO_2(APTMS) nanoparticles for dysprosium adsorption. J Hazard Mater 378:120764

Kim J, Sadasivuni KK, Zhai L, Gao X, Jo EB (2014) Cellulose nanocrystals and nanofibers for smart optics materials. Int Sym Optomechatr Technol 2014:330–332

Kontturi E, Laaksonen P, Linder MB, Groschel AH, Rojas OJ, Ikkala O (2018) Advanced Materials through Assembly of Nanocelluloses. Adv Mater 30:e1703779

Liang XD, Ye M, Yang L, Fu WB, Li Z (2018) Evaluation and policy research on the sustainable development of china's rare earth resources. Sustainability 10:16

Long LY, Weng YX, Wang YZ (2018) Cellulose aerogels: synthesis, applications, and prospects. Polymers 10:623

Mahdi Z, Yu QJ, El Hanandeh A (2018) Competitive adsorption of heavy metal ions (Pb^{2+}, Cu^{2+}, and Ni^{2+}) onto date seed biochar: batch and fixed bed experiments. Sep Sci and Technol 54:888–901

Ni'am AC, Wang YF, Chen SW, Chang GM, You SJ (2020) Simultaneous recovery of rare earth elements from waste permanent magnets (WPMs) leach liquor by solvent extraction and hollow fiber supported liquid membrane. Chem Eng Process 148:107831

Peng Y, Gardner DJ, Han Y (2011) Drying cellulose nanofibrils: in search of a suitable method. Cellulose 19:91–102

Prodius D, Gandha K, Mudring AV, Nlebedim IC (2020) Sustainable urban mining of critical elements from magnet and electronic wastes. ACS Sustain Chem Eng 8:1455–1463

Salimian S, Zadhoush A, Naeimirad M, Kotek R, Ramakrishna S (2018) A review on aerogel: 3D nanoporous structured fillers in polymer-based nanocomposites. Polym Compos 39:3383–3408

Sato K, Mochizuki H, Okajima K, Yamane C (2004) Effects of hydrophobic solvents on X-Ray diffraction patterns of regenerated cellulose membrane. Polym 36:478–482

Stepanova M, Averianov I, Gofman I, Solomakha O, Nashchekina Y, Korzhikov-Vlakh V, Korzhikova-Vlakh E (2019) Poly(ε-caprolactone)-based biocomposites reinforced with nanocrystalline cellulose grafted with poly(L-lactic acid). IOP Conf Ser: Materi Sci Eng 500:012021

Sun D, Zhu Y, Meng M, Qiao Y, Yan Y, Li C (2017) Fabrication of highly selective ion imprinted macroporous membranes with crown ether for targeted separation of lithium ion. Sep Purif Technol 175:19–26

Wang L, Zhao X, Zhang J, Xiong Z (2017) Selective adsorption of Pb (II) over the zinc-based MOFs in aqueous solution-kinetics, isotherms, and the ion exchange mechanism. Environ Sci Pollut Res 24:14198–14206

Xu YT, Dai Y, Nguyen TD, Hamad WY, MacLachlan MJ (2018) Aerogel materials with periodic structures imprinted with cellulose nanocrystals. Nanoscale 10:3805–3812

Zhang J, Zhang J (2020) Advanced functional materials based on cellulose. Acta Polym Sin 10(8):1376–1398

Zhang L, Li L, Shi D, Peng X, Song F, Nie F (2019) Kinetics and mechanism study of lithium extraction from alkaline solution by HFTA and TOPO and stripping process using Lewis cell technique. Sep Purif Technol 211:917–924

Zhang Y, Bian T, Jiang R, Zhang Y, Zheng X, Li Z (2021) Bionic chitosan-carbon imprinted aerogel for high selective recovery of Gd(III) from end-of-life rare earth productions. J Hazard Mater 407:124347

Zhao F, Repo E, Song Y, Yin D, Hammouda SB, Chen L, Kalliola S, Tang J, Tam KC, Sillanpää M (2017) Polyethylenimine-cross-linked cellulose nanocrystals for highly efficient recovery of rare earth elements from water and a mechanism study. Green Chem 19:4816–4828

Zhao H, Xia J, Yin D, Luo M, Yan C, Du Y (2019) Rare earth incorporated electrode materials for advanced energy storage. Coord Chem Rev 390:32–49

Zheng X, Liu E, Zhang F, Yan Y, Pan J (2016) Efficient adsorption and separation of dysprosium from NdFeB magnets in an acidic system by ion imprinted mesoporous silica sealed in a dialysis bag. Green Chem 18:5031–5040

Zheng X, Zhang Y, Bian T, Wang D, Li Z (2019) One-step fabrication of imprinted mesoporous cellulose nanocrystals films for selective separation and recovery of Nd(III). Cellulose 26:5571–5582

Zheng XD, Zhang Y, Bian TT, Zhang YZ, Li ZY, Pan JM (2020) Oxidized carbon materials cooperative construct ionic imprinted cellulose nanocrystals films for efficient adsorption of Dy(III). Chem Eng J 381:10

Zhu Y, Niu Y, Li H, Ren B, Qu R, Chen H, Zhang Y (2018) Removal of Cd(II) and Fe(III) from DMSO by silica gel supported PAMAM dendrimers: Equilibrium, thermodynamics, kinetics and mechanism. Ecotoxicol Environ Saf 162:253–260